

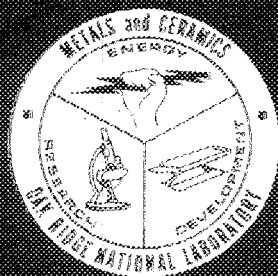
ORNL-5077

Cy 2

MARTIN MARIETTA ENERGY SYSTEMS LIBRARIES



3 4456 0285182 1



Scaling Relations for Eddy Current Phenomena

C. V. Dodd W. E. Deeds

OAK RIDGE NATIONAL LABORATORY
CENTRAL RESEARCH LIBRARY
DOCUMENT COLLECTION

LIBRARY LOAN COPY

DO NOT TRANSFER TO ANOTHER PERSON

If you wish someone else to see this document, send in name with document and the library will arrange a loan.



OAK RIDGE NATIONAL LABORATORY

OPERATED BY UNION CARBIDE CORPORATION • FOR THE U.S. ATOMIC ENERGY COMMISSION

Printed in the United States of America. Available from
National Technical Information Service
U.S. Department of Commerce
5285 Port Royal Road, Springfield, Virginia 22161
Price: Printed Copy \$4.00; Microfiche \$2.25

This report was prepared as an account of work sponsored by the United States Government. Neither the United States nor the Energy Research and Development Administration, nor any of their employees, nor any of their contractors, subcontractors, or their employees, makes any warranty, express or implied, or assumes any legal liability or responsibility for the accuracy, completeness or usefulness of any information, apparatus, product or process disclosed, or represents that its use would not infringe privately owned rights.

ORNL-5077
UC-20 — Controlled Thermonuclear
Processes and Plasma Physics

Contract No. W-7405-eng-26

METALS AND CERAMICS DIVISION

SCALING RELATIONS FOR EDDY CURRENT PHENOMENA

C. V. Dodd and W. E. Deeds

NOVEMBER 1975

OAK RIDGE NATIONAL LABORATORY
Oak Ridge, Tennessee 37830
operated by
UNION CARBIDE CORPORATION
for the
U.S. ENERGY RESEARCH AND DEVELOPMENT ADMINISTRATION



3 4456 0285182 1

ACKNOWLEDGMENTS

The authors would like to express their appreciation to H. T. Yeh, W. A. Simpson, K. Kawashima, and R. W. McClung for their review of this report and their many helpful suggestions. They would also like to express their gratitude to Grace Seals, Word Processing, Technical Publications Department, for the typing and preparation of this report.

CONTENTS

	<u>Page</u>
Introduction	1
I. Single Frequency, Scaled Equations for the Vector Potential . .	3
II. Fourier Synthesis to form Non-Sinusoidal Pulses	7
III. Physical Phenomena	9
A. Eddy Current Density	9
B. Eddy Current Power	10
C. Magnetic Field	11
D. Force Density	13
E. Voltages Induced in Coupled Circuits	15
F. Currents in Multiple Coupled Circuits	18
G. Driving Voltages	22
IV. Measurements of the Various Properties	24
A. Eddy Current Density	24
B. Eddy Current Power	24
C. Magnetic Field	25
D. Force Density	25
E. Voltages in Circuits	25
V. Use of Measurements and Scaling in Lieu of Calculations	26
A. Advantages of Measurements	26
B. Advantages of Calculations	26
VI. Experimental Verification of Scaling	27
VII. Summary and Conclusions	33
References	35

SCALING RELATIONS FOR EDDY CURRENT PHENOMENA*

C. V. Dodd and W. E. Deeds**

Metals and Ceramics Division
Oak Ridge National Laboratory

Abstract

Formulae are given for various electromagnetic quantities for coils in the presence of conductors, with the scaling parameters factored out so that small-scale model experiments can be related to large-scale apparatus. Particular emphasis is given to such quantities as eddy current heating, forces, power, and induced magnetic fields. For axially symmetric problems, closed-form integrals are available for the vector potential and all the other quantities obtainable from it. For unsymmetrical problems, a three-dimensional relaxation program can be used to obtain the vector potential and then the derivable quantities. Data on experimental measurements are given to verify the validity of the scaling laws for forces, inductances, and impedances. Indirectly these also support the validity of the scaling of the vector potential and all of the other quantities obtained from it.

Introduction

Scaling of eddy current nondestructive testing problems has been used for many years, for both analytical calculations and experimental measurements.¹⁻⁷ In the analytical calculations, we reduce the configuration to dimensionless ratios, perform all the calculations using pure numbers, and only introduce dimensions in the final step. In the experimental measurements, we perform the measurements on models that are usually larger than the actual test so that the dimensions can be more accurately controlled.

*Funding provided by the Superconducting Magnet Development Program of the Thermonuclear Division.

**Consultant from The University of Tennessee, Knoxville, Tennessee.

We have started our analysis with the vector potential, and can obtain closed form integral equations for it for many of the simpler cases. These equations can be quickly evaluated on a small digital computer.

For more complicated problems we must use a relaxation or finite difference technique, in either 2 or 3 dimensions. This technique requires a large digital computer for numerical evaluation. Once the vector potential has been determined for various discrete frequencies it can be calculated for any piece-wise continuous wave-shape using Fourier synthesis. From the vector potential any induction phenomenon can be calculated. These calculations generally involve the numerical evaluation of multiple integrals which involve functions of the vector potential. As an alternative to numerical calculations, in many instances we can use measurements on a model to evaluate the multiple integrals.

A number of successful designs have been completed using these techniques.⁸⁻¹³

I. Single Frequency, Scaled Equations for the Vector Potential

An axially symmetric coil of rectangular cross-section above multiple parallel planes is shown in Fig. 1. The closed form integral equation for the vector potential produced by such a coil is, in the n -th region:

$$A^n(r, z) = NI\mu_0 \left\{ \left[\frac{1}{2(R_2 - R_1)L_3} \right] \int_0^\infty \frac{J(R_2, R_1)J_1(\alpha r)}{\alpha^3 V_{22}(k, 1)} e^{-\alpha(L_2 + L_6)} \right. \\ \left. \times [1 - e^{-\alpha L_3}] [V_{12}(n, 1)e^{-\alpha z} + V_{22}(n, 1)e^{\alpha z}] d\alpha \right\}. \quad (1)$$

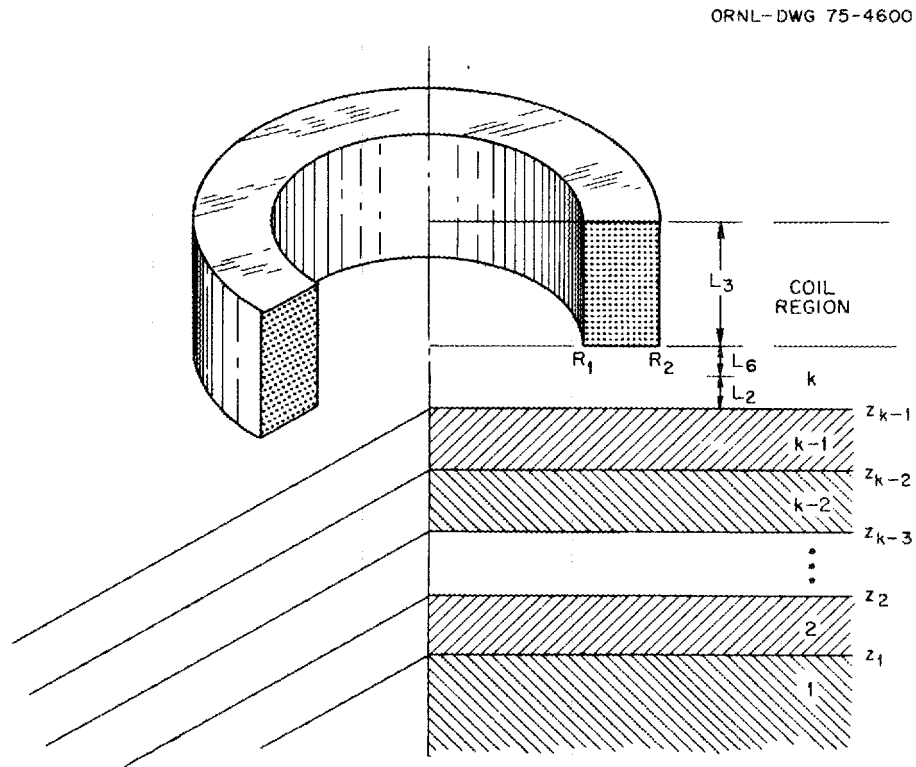


Fig. 1. Coil Above Multiple Planes.

The terms in brackets are completely dimensionless. They are a function of the linear dimensions divided by scaling factor (usually the mean radius of a coil of interest, R_5). The frequency enters only through the function $\omega\mu\sigma R_5^2$, which is also dimensionless and would usually be kept constant in scaling a model. The terms containing the frequency are:

$$\alpha_n = \sqrt{\alpha^2 + j\omega\mu_n\sigma_n R_5^2} \quad , \quad (2)$$

and

$$\beta_n = \frac{1}{\mu_{nrel}} \sqrt{\alpha^2 + j\omega\mu_n\sigma_n R_5^2} \quad . \quad (3)$$

Both of these terms are dimensionless.

The terms $\frac{V_{12}(n,1)}{V_{22}(k,1)}$ contain an equal number of β_n 's in both the

numerator and denominator and are dimensionless.

We can also obtain the vector potential for any irregular coils and conductors using a three-dimensional relaxation technique. Using Cartesian coordinates, as shown in Fig. 2, we find for the three components of the vector potential in non-ferromagnetic media:

$$\begin{aligned} A_{x_{klm}} = & \left[\mu_0 NI \frac{\delta_e \cos \alpha_x}{n^2 (R_2 - R_1) L_3} + \frac{\sigma_k}{\sigma_{k+1}} A_{x_{k+1}} + A_{x_{k-1}} + A_{x_{l+1}} + A_{x_{l-1}} \right. \\ & \left. + A_{x_{m+1}} + A_{x_{m-1}} + \left(\frac{\sigma_k}{\sigma_{k+1}} - 1 \right) \left(A_{y_{l+1}} - A_{y_l} + A_{z_{m+1}} - A_{z_m} \right) \right] \\ & \div \left[5 + \frac{\sigma_k}{\sigma_{k+1}} + \frac{j\omega\mu\sigma_{klm} R_5^2}{n^2} \right] \quad , \quad (4) \end{aligned}$$

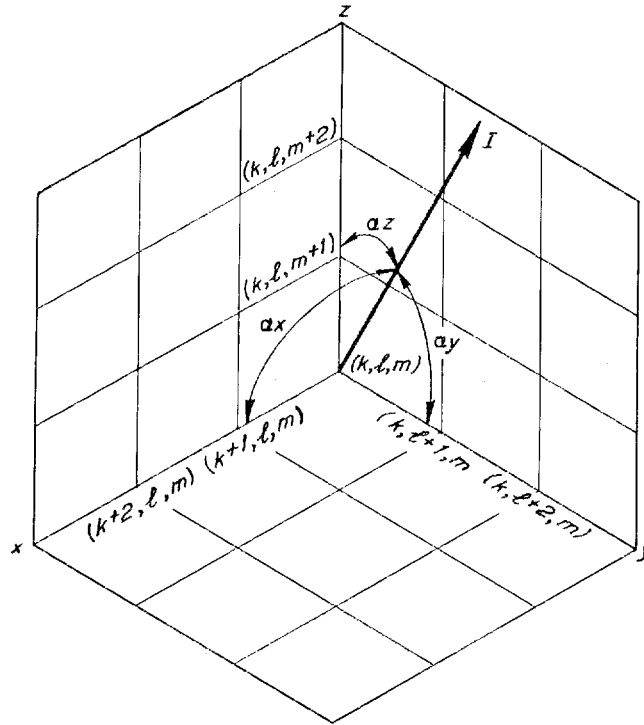


Fig. 2. Cartesian Coordinates for Three-Dimensional Relaxation.

$$\begin{aligned}
 A_{y_{klm}} = & \left[\mu_0 N I \frac{\delta_c \cos \alpha_y}{n^2 (R_2 - R_1) L_3} + \frac{\sigma_l}{\sigma_{l+1}} A_{y_{l+1}} + A_{y_{l-1}} + A_{y_{m+1}} + A_{y_{m-1}} \right. \\
 & \left. + A_{y_{k+1}} + A_{y_{k-1}} + \left(\frac{\sigma_l}{\sigma_{l+1}} - 1 \right) \left(A_{z_{m+1}} - A_{z_m} + A_{x_{k+1}} - A_{x_k} \right) \right] \\
 & \div \left[5 + \frac{\sigma_l}{\sigma_{l+1}} + \frac{j \omega \mu \sigma_{klm} R_5^2}{n^2} \right], \quad (5)
 \end{aligned}$$

$$\begin{aligned}
A_{z_{klm}} = & \left[\mu_0 N I \frac{\delta_c \cos \alpha_z}{n^2 (R_2 - R_1) L_3} + \frac{\sigma_m}{\sigma_{m+1}} A_{z_{m+1}} + A_{z_{m-1}} + A_{z_{k+1}} + A_{z_{k-1}} + A_{z_{l+1}} + A_{z_{l-1}} \right. \\
& \left. + \left(\frac{\sigma_m}{\sigma_{m+1}} - 1 \right) \left(A_{x_{k+1}} - A_{x_k} + A_{y_{l+1}} - A_{y_l} \right) \right] \\
& \div \left[5 + \frac{\sigma_m}{\sigma_{m+1}} + \frac{j\omega\mu\sigma_{klm} R_5^2}{n^2} \right], \tag{6}
\end{aligned}$$

where

μ_0 is the magnetic permeability of free space ($4\pi \times 10^{-7}$),

N is the number of turns in the coil,

I is the current per turn, and any subscript not written is assumed to be k, l, m , as the case might be.

All other terms are dimensionless, and the vector potential is directly proportional to the source terms, $\mu_0 N I$. The quantity δ_c is equal to 1 if the lattice point is inside the coil, zero if it is outside. α_x is the angle between the wire direction and the x axis; R_5 is the coil mean radius; n is the number of lattice points in the coil mean radius R_5 ; N_x is the number of lattice points in the coil as the coil passes through the plane perpendicular to the x -axis; and the term $\omega\mu\sigma_{klm} R_5^2$ is dimensionless.

From these equations, the vector potential at each point can be obtained using a relaxation process.

The dimensionless numerical answer so determined will depend on:

1. The coil and conductor geometry;
2. The value of $\omega\mu\sigma R_5^2$.

The dimensioned factors multiplying the dimensionless numerical answer will be $\mu_0 NI$.

II. Fourier Synthesis to Form Non-Sinusoidal Pulses

Thus far, the vector potential for a single frequency, ω , has been obtained. We shall now superpose a number of different frequencies to obtain the vector potential of a pulse, such as illustrated in Fig. 3, by Fourier synthesis. If the current is piecewise continuous and has a repetition period T , we can write the current waveform as

$$I(\tau) = I_0 \left\{ \frac{\alpha_0}{2} + \sum_{m=1}^{\infty} \alpha_m \cos(m\omega_1\tau) + b_m \sin(m\omega_1\tau) \right\}, \quad (7)$$

where $\omega_1 = 2\pi/T$,

$$\alpha_m = \frac{\omega_1}{\pi} \int_{-T/2}^{T/2} \frac{I(\tau)}{I_0} \cos(m\omega_1\tau) d\tau \quad m = 0, 1, 2, 3 \dots \infty, \quad (8)$$

and

$$b_m = \frac{\omega_1}{\pi} \int_{-T/2}^{T/2} \frac{I(\tau)}{I_0} \sin(m\omega_1\tau) d\tau \quad m = 1, 2, 3 \dots \infty. \quad (9)$$

ORNL-DWG 75-6863

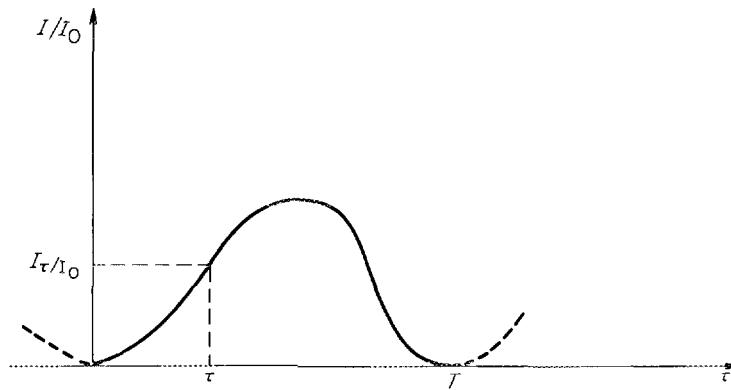


Fig. 3. Diagram of Current Pulse.

From the current, the vector potential as a function of time can be calculated:

$$A(\tau) = \mu_0 I_0 N \left\{ \frac{\alpha_0}{2} \bar{A}(0) + \sum_{m=1}^{\infty} \alpha_m \bar{A}(m) \cos(m\omega_1 \tau + \phi_m) + b_m \bar{A}(m) \sin(m\omega_1 \tau + \phi_m) \right\}, (10)$$

where $\bar{A}(m)$ is the vector potential calculated at the angular frequency $m\omega_1$ with the $\mu_0 I_0 N$ factored out. $\bar{A}(m)$ is completely dimensionless and

depends only on the geometry and the values of the products $m\omega_1\mu\sigma R_5^2$. The value of ω_1 can be varied to compensate for changes in σ and R_5 . The value of τ must then be varied so that the product $\omega_1\tau$ is constant. Thus, the pulse in real time t may vary for the scaled model. The phase shift, ϕ_m , is determined by $\phi_m = \alpha \tan\left(\frac{ImA}{RLA}\right)$, and $\bar{A}(m) = [RLA^2(m) + Im A^2(m)]^{1/2}$. We shall rewrite the equation for $A(\tau)$ as

$$A(\tau) = \mu_0 IN \bar{A}(\tau),$$

where

$\bar{A}(\tau)$ is the dimensionless sum given in curly brackets in Eq. (10).

From the vector potential we can calculate all the physically observable phenomena.

III. Physical Phenomena

A. Eddy Current Density

$$\vec{J} = \sigma \vec{E} = -\sigma \frac{\partial \vec{A}}{\partial \tau}. \quad (11)$$

$$\vec{J} = \sigma \mu_0 I_0 N \omega_1 \sum_{m=1}^{\infty} m \bar{A}(m) [a_m \sin(m\omega_1\tau + \phi_m) - b_m \cos(m\omega_1\tau + \phi_m)]. \quad (12)$$

The total current passing through a normalized area, dA_n , in terms of the actual area, $dA' = (dA'/R_5^2)R_5^2 = dA_n R_5^2$, is given by

$$\vec{J}_A = I_0 N dA_n (\omega_1 \mu_0 \sigma R_5^2) \sum_{m=1}^{\infty} m \vec{A}(m) [\alpha_m \sin(m\omega_1 \tau + \phi_m) - b_m \cos(m\omega_1 \tau + \phi_m)] . \quad (13)$$

The only dimensions are contained in the I_0 . All the other terms are dimensionless and normalized.

B. Eddy Current Power

The eddy current power dissipated per unit volume is:

$$\frac{dP}{dV} = \vec{J} \cdot \vec{E} = \sigma \left(\frac{\partial A}{\partial \tau} \right)^2 . \quad (14)$$

The instantaneous power dissipated in a normalized volume, dV_n , is

$$P = I_0^2 N^2 \omega_1 \mu_0 R_5 dV_n (\omega_1 \mu_0 \sigma R_5^2) \times \left\{ \sum_{m=1}^{\infty} m \vec{A}(m) [b_m \cos(m\omega_1 \tau + \phi_m) - \alpha_m \sin(m\omega_1 \tau + \phi_m)] \right\}^2 . \quad (15)$$

Again, all dimensions are contained in the terms $I_0^2 \omega_1 \mu_0 R_5$, and the others are dimensionless.

If there are several different components of the vector potential, the total power will contain the sum of the squares of the time derivatives of all of the components of the vector potential. That is:

$$\frac{dP}{dV} = \sigma \left\{ \left(\frac{\partial A_x}{\partial \tau} \right)^2 + \left(\frac{\partial A_y}{\partial \tau} \right)^2 + \left(\frac{\partial A_z}{\partial \tau} \right)^2 \right\} . \quad (16)$$

C. Magnetic Field

$$\vec{B} = \nabla \times \vec{A} \quad (17)$$

The exact form of the curl of \vec{A} depends on the coordinate system in which \vec{A} and \vec{B} are computed. Using symbols defined by Morse & Feshbach and shown in Fig. 4, we have:

$$\vec{B} = \nabla \times \vec{A} = \frac{1}{h_1 h_2 h_3} \sum_{j,k,l} h_j \hat{a}_j \left[\frac{\partial}{\partial \xi_k} (h_l A_l) - \frac{\partial}{\partial \xi_l} (h_k A_k) \right] . \quad (18)$$

The dimensions of \vec{B} will be \vec{A}/length .

In general, we will have for the components of the magnetic field:

$$B_j = \mu_0 I_0 N \frac{h_j}{h_1 h_2 h_3} \left[\frac{\partial}{\partial \xi_k} \left(h_l \bar{A}_l(\tau) \right) - \frac{\partial}{\partial \xi_l} \left(h_k \bar{A}_k(\tau) \right) \right] . \quad (19)$$

If we normalize the dimensions by dividing all lengths by R_5 we have

$$B_j = \frac{\mu_0 I_0 N}{R_5} \frac{h_j}{h_1 h_2 h_3} \left[\frac{\partial}{\partial \xi_k} \left(h_l \bar{A}_l(\tau) \right) - \frac{\partial}{\partial \xi_l} \left(h_k \bar{A}_k(\tau) \right) \right] . \quad (20)$$

ORNL-DWG 75-6864

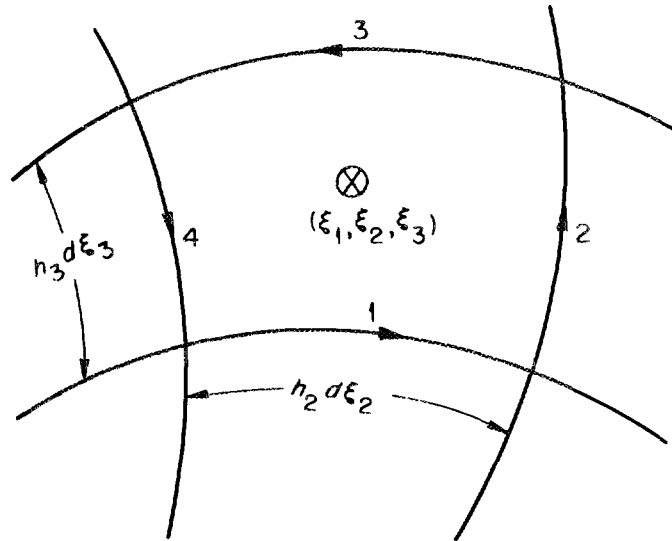


Fig. 4. Curl in Curvilinear Coordinates.

For the special case of an axially symmetric coil above plane layers of conductor as shown in Fig. 1 with only a θ -component of the vector potential, the expressions for the Z -component of the magnetic field in the n -th region (in terms of the variables used in the computer program) is:

$$B_z^n(r, z) = \frac{N_3 I_9 \mu_0}{2(R_2 - R_1) L_3 R_5} \int_0^\infty \frac{e^{-\alpha L_6} e^{-\alpha L_2}}{\alpha^2} J(R_2, R_1) [1 - e^{-\alpha L_3}]$$

$$\times J_0(\alpha r) \left\{ \frac{V_{12}(n, 1)}{V_{22}(k, 1)} e^{-\alpha_n z} + \frac{V_{22}(n, 1)}{V_{22}(k, 1)} e^{\alpha_n z} \right\} d\alpha . \quad (21)$$

The r component is given by:

$$B_r^n(r, z) = \frac{N_3 I_9 \mu_0}{2(R_2 - R_1) L_3 R_5} \int_0^\infty \frac{e^{-\alpha L_6} e^{-\alpha L_2}}{\alpha^3} J(R_2, R_1) [1 - e^{-\alpha L_3}]$$

$$\times J_1(\alpha r) \left\{ -\frac{V_{12}(n, 1)}{V_{22}(k, 1)} \alpha_n e^{-\alpha_n z} + \frac{V_{22}(n, 1)}{V_{22}(k, 1)} \alpha_n e^{\alpha_n z} \right\} d\alpha . \quad (22)$$

D. Force Density

For non-ferromagnetic materials we have for the force density:

$$\frac{d\vec{F}}{dV} = \vec{J} \times \vec{B} = -\sigma \frac{\partial \vec{A}}{\partial \tau} \times (\nabla \times \vec{A}) . \quad (23)$$

For the j th component of force in a normalized volume

$$dV_n = h_1 h_2 h_3 d\xi_1 d\xi_2 d\xi_3 \quad \text{we have}$$

$$\begin{aligned}
dF_j = & \mu_0 I_0^2 N^2 (\omega_1 \mu_0 \sigma R_5^2) \left\{ \left[\sum_{m=1}^{\infty} m \bar{A}_k(m) [\alpha_m \sin(m\omega_1\tau + \phi_m) \right. \right. \\
& \left. \left. - b_m \cos(m\omega_1\tau + \phi_m)] \right] h_z \left[\frac{\partial}{\partial \xi_j} \left(h_k \bar{A}_k(\tau) \right) - \frac{\partial}{\partial \xi_k} \left(h_j \bar{A}_j(\tau) \right) \right] \right. \\
& \left. - \left[\sum_{m=1}^{\infty} m \bar{A}_z(m) [\alpha_m \sin(m\omega_1\tau + \phi_m) - b_m \cos(m\omega_1\tau + \phi_m)] \right] \right. \\
& \left. \times h_k \left[\frac{\partial}{\partial \xi_z} \left(h_j \bar{A}_j(\tau) \right) - \frac{\partial}{\partial \xi_j} \left(h_z \bar{A}_z(\tau) \right) \right] \right\} d\xi_1 d\xi_2 d\xi_3 . \quad (24)
\end{aligned}$$

The only dimensions are contained in the $\mu_0 I_0^2 N^2$ term. The α_m and b_m terms depend on the relative pulse shape, and the $A(i)$ terms depend on the geometrical shape and the dimensionless numbers, $m\omega_1 \mu_0 \sigma R_5^2$.

If we evaluate the z component of force in cylindrical coordinates we have:

$$\begin{aligned}
dF_z = & \mu_0 I_0^2 N^2 (\omega_1 \mu_0 \sigma R_5^2) \left\{ \left[\sum_{m=1}^{\infty} m \bar{A}_r(m) [\alpha_m \sin(m\omega_1\tau + \phi_m) \right. \right. \\
& \left. \left. - b_m \cos(m\omega_1\tau + \phi_m)] \right] r \left[\frac{\partial}{\partial z} \bar{A}_r(\tau) - \frac{\partial}{\partial r} \bar{A}_z(\tau) \right] \right. \\
& \left. - \left[\sum_{m=1}^{\infty} m \bar{A}_\theta(m) [\alpha_m \sin(m\omega_1\tau + \phi_m) - b_m \cos(m\omega_1\tau + \phi_m)] \right] \right. \\
& \left. \times \left[\frac{\partial}{\partial \theta} \bar{A}_z(\tau) - \frac{\partial}{\partial z} \left(r \bar{A}_\theta(\tau) \right) \right] \right\} dr d\theta dz . \quad (25)
\end{aligned}$$

E. Voltages Induced in Coupled Circuits

The voltage induced in a length of wire is

$$V = \int \frac{\partial \vec{A}}{\partial t} \cdot d\vec{S}. \quad (26)$$

The general expression for the voltage induced in coil 1 by a current I_2 flowing in coil 2, as shown in Fig. 5, is:

$$V_{12} = \mu_0 I_2 N_2 \omega_1 R_5 \sum_{m=1}^{\infty} m [\alpha_m \sin (m\omega_1 \tau + \phi_{12m}) - b_m \cos (m\omega_1 \tau + \phi_{12m})] \left| \int_{\text{all turns in coil 1}} \vec{A}_2(j\omega_1 m) \cdot d\vec{S}_1 \right|, \quad (27)$$

where

$$\phi_{12m} = \text{atan} \left(\frac{\text{Im} \int_1 \vec{A}_2(j\omega_1 m) \cdot d\vec{S}_1}{\text{Re} \int_1 \vec{A}_2(j\omega_1 m) \cdot d\vec{S}_1} \right), \quad (28)$$

and the element of length, $d\vec{S}_1$, has been normalized. Hence, the mutual inductance of the two coils is:

$$M_{12} = \frac{V_{12}}{I_2} = \mu_0 N_2 \omega_1 R_5 \sum_{m=1}^{\infty} m [\alpha_m \sin (m\omega_1 \tau + \phi_{12m}) - b_m \cos (m\omega_1 \tau + \phi_{12m})] \times \left| \sum_{j,k,l} \int_{\text{all turns in coil 1}} A_{l2}(j\omega_1 m) dS_l \right|. \quad (29)$$

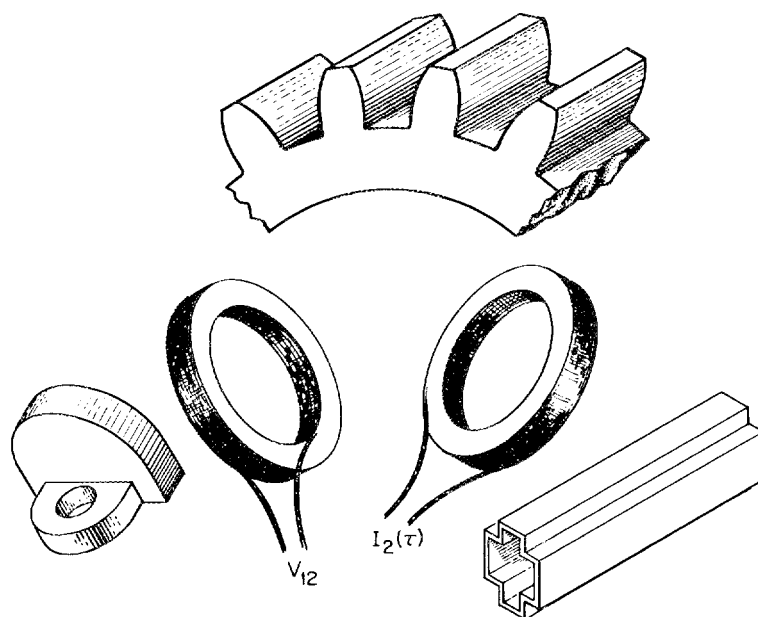


Fig. 5. Coils in the Presence of Arbitrary Conductors.

The term in the absolute value brackets must be integrated over all of the turns in coil 1. However, if the coil has a constant turns density over its cross-section we can simplify the term to:

$$\int_{\text{all turns in coil 1}} \vec{A}_2(j\omega_1 m) \cdot d\vec{S} = \sum_{\text{turns}} \int_{\text{single turn}} \vec{A}_2(j\omega_1 m) \cdot d\vec{S} \quad (30)$$

$$\approx \frac{N_1}{\text{cross sectional area}_1} \iint_{\text{c.s. area}_1} \int \vec{A}_2(j\omega_1 m) \cdot d\vec{S} d(\text{c.s. area}_1) .$$

Therefore,

$$M_{12} = \mu_0 N_1 N_2 \omega_1 R_5 \sum_{m=1}^{\infty} m [\alpha_m \sin(m\omega_1 \tau + \phi_{12m}) - b_m \cos(m\omega_1 \tau + \phi_{12m})] \\ \times \frac{1}{A_1} \left| \sum_{j,k,l} \iiint_{A_1} \bar{A}_{k2}(j\omega_1 m) dS_k dA_1 \right|, \quad (31)$$

where A_1 is the cross-sectional area of the coil, perpendicular to the direction of the turns. The dimensions of A_1 will cancel those of dA_1 . For consistency we shall take both to be normalized. If dS is taken along one coordinate, the summation over l, m and r reduces to

$$\iiint_{\text{coil volume}} A_{l2}(j\omega_1 m) d(\text{Vol}). \quad (32)$$

The value of M_{12} , in ohms, is directly proportional to $\mu_0 N_2 \omega_1 R_5$. All of the other terms are dimensionless and depend upon the relative geometry and the shape of the current wave form. The voltage induced in the q th circuit due to current flowing in N other circuits can be calculated by the equation,

$$V_q = \sum_{r=1}^N M_{qr} I_r + I_q R_q. \quad (33)$$

Furthermore the terms in the expression can be written as

$$V_q = \sum_r^N \mu_0 I_r^N N_q^N \omega_1 R_5 \sum_{m=1}^{\infty} m \left[\alpha_m \sin(m\omega_1\tau + \phi_{mqr}) - b_m \cos(m\omega_1\tau + \phi_{mqr}) \right] \left| \frac{1}{A_q} \iiint_{vol_q} \bar{A}_r(j\omega_1 m) d Vol \right| + I_q^R \cdot \quad (34)$$

F. Currents in Multiple Coupled Circuits

We shall define a coupling coefficient with the following equation:

$$C_{mqr} = \frac{\mu_0 N_q^N N_r^N \omega_1 R_5}{A_q} \left| \iiint_{vol_q} \bar{A}_r(j\omega_1 m) d Vol \right| \quad (35)$$

and define the α_m coefficient for the current in the r th coil as

$$\alpha_{rm} = \alpha_m \cdot \quad (36)$$

The current loop equation for the q th loop for N coils then becomes:

$$V_q(\tau) = A_{q0} I_q^R + \sum_{r=1}^N \sum_{m=1}^N I_r \left\{ \alpha_{rm} \left[R_q \delta_{qr} \sin(m\omega_1\tau) + C_{mqr} \sin(m\omega_1\tau + \phi_{mqr}) \right] + b_{rm} \left[R_q \delta_{qr} \cos(m\omega_1\tau) + C_{mqr} \cos(m\omega_1\tau + \phi_{mqr}) \right] \right\} \cdot \quad (37)$$

We have assumed that the current wave shapes can be represented by a finite number of terms, N' . We can use the orthogonal properties of the trigonometric functions to solve for the a_{rm} and b_{rm} coefficients. We shall multiply eq. (37) by $\sin(n\omega_1\tau)$, integrate from 0 to T (the period of the periodic function, $T = 2\pi/\omega_1$), and use the following relationships to simplify the equations:

$$\sin(m\omega_1\tau + \phi_{mqr}) = \sin(m\omega_1\tau) \cos(\phi_{mqr}) + \cos(m\omega_1\tau) \sin(\phi_{mqr}) \quad (38)$$

$$\cos(m\omega_1\tau + \phi_{mqr}) = \cos(m\omega_1\tau) \cos(\phi_{mqr}) - \sin(m\omega_1\tau) \sin(\phi_{mqr}) \quad (39)$$

$$\int_0^{2\pi/\omega_1} \sin(m\omega_1\tau) \sin(n\omega_1\tau) d\tau = \frac{T}{2} \delta_{mn} = \frac{\pi}{\omega_1} \delta_{mn} \quad (40)$$

$$\int_0^{2\pi/\omega_1} \cos(m\omega_1\tau) \cos(n\omega_1\tau) d\tau = \frac{T}{2} \delta_{mn} = \frac{\pi}{\omega_1} \delta_{mn} \quad (41)$$

$$\int_0^{2\pi/\omega_1} \sin(m\omega_1\tau) \cos(n\omega_1\tau) d\tau = 0. \quad (42)$$

Using these relationships, we obtain:

$$\begin{aligned} \sum_{r=1}^N \left[I_r A_{rm} (R_q \delta_{qr} + C_{mqr} \cos \phi_{mqr}) + I_r b_{rm} (-C_{mqr} \sin \phi_{mqr}) \right] \\ = \frac{\omega_1}{\pi} \int_0^T V_q(\tau) \sin(m\omega_1\tau) d\tau. \end{aligned} \quad (43)$$

Similarly, if we multiply eq. (37) by $\cos(m\omega_1\tau)$ and integrate from 0 to $2\pi/\omega_1$, we can obtain:

$$\begin{aligned} \sum_{r=1}^N \left[I_r a_{rm} (C_{mqr} \sin \phi_{mqr}) + I_r b_{rm} (R_q \delta_{qr} + C_{mqr} \cos \phi_{mqr}) \right] \\ = \frac{\omega_1}{\pi} \int_0^T V_q(\tau) \cos(m\omega_1\tau) d\tau . \end{aligned} \quad (44)$$

For each angular frequency component, $m\omega_1$, there will be N equations of the form of eq. (43), one for each of the N coils, designated by q :

$$\begin{aligned} I_1 a_{1m} (R_1 + C_{m11} \cos \phi_{m11}) + \dots + I_n a_{nm} (C_{m1n} \cos \phi_{m1n}) \\ + I_1 b_{1m} (-C_{m11} \sin \phi_{m11}) + \dots + I_n b_{nm} (-C_{m1n} \sin \phi_{m1n}) \\ \vdots \\ = \frac{\omega_1}{\pi} \int_0^T V_1(\tau) \sin(m\omega_1\tau) d\tau \end{aligned} \quad (45)$$

$$\begin{aligned} I_1 a_{1m} (C_{mn1} \cos \phi_{mn1}) + \dots + I_n a_{nm} (R_n + C_{mnn} \cos \phi_{mnn}) \\ + I_1 b_{1m} (-C_{mn1} \sin \phi_{mn1}) + \dots + I_n b_{nm} (-C_{mnn} \sin \phi_{mnn}) \\ = \frac{\omega_1}{\pi} \int_0^T V_n(\tau) \sin(m\omega_1\tau) d\tau . \end{aligned}$$

There will also be N equations of the form of eq. (44), one for each of the N coils:

$$\begin{aligned}
 & I_1 \alpha_{1m} (C_{m11} \sin \phi_{m11}) + \dots + I_n \alpha_{nm} (C_{m1n} \sin \phi_{m1n}) \\
 & + I_1 b_{1m} (R_1 + C_{m11} \cos \phi_{m11}) + \dots + I_n b_{nm} (C_{m1n} \cos \phi_{m1n}) \\
 & = \frac{\omega_1}{\pi} \int_0^T V_1(\tau) \cos(m\omega_1\tau) d\tau . \\
 & \vdots \tag{46}
 \end{aligned}$$

$$\begin{aligned}
 & I_1 \alpha_{1m} (C_{mn1} \sin \phi_{mn1}) + \dots + I_n \alpha_{nm} (C_{mnn} \sin \phi_{mnn}) \\
 & + I_1 b_{1m} (C_{mn1} \cos \phi_{mn1}) + \dots + I_n b_{nm} (R_n + C_{mnn} \cos \phi_{mnn}) \\
 & = \frac{\omega_1}{\pi} \int_0^T V_n(\tau) \cos(m\omega_1\tau) d\tau .
 \end{aligned}$$

Equations (45) and (46) provide $2N$ linearly independent equations to determine the $2N$ coefficients, $I_1 \alpha_{1m}, \dots, I_n \alpha_{nm}, I_1 b_{1m}, \dots, I_n b_{nm}$, for the single frequency component, $m\omega_1$. A similar set of $2N$ equations must be solved for each of the frequency components in the pulse.

The d.c. component of current in the q -th coil will be

$$\frac{\alpha_{q0} I_q}{2} = \frac{\omega_1}{4\pi R_q} \int_0^T V_q(\tau) d\tau . \tag{47}$$

There will be just N equations of this type to be solved.

G. Driving Voltages

In equations (43) through (47), it is assumed that the voltage $V_q(\tau)$ applied to the q -th coil is a known function of time, as is usually the case. For the charge-up of a coil, the voltage would be a ramp function, as shown in Fig. 6.

ORNL-DWG 75-10666

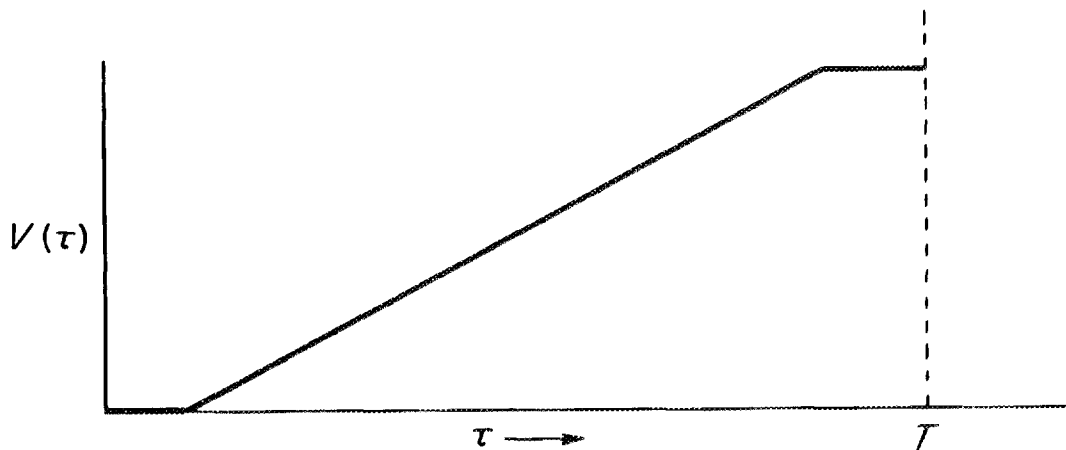


Fig. 6. Charging a Coil with a Voltage Ramp.

We can also simulate the turn off of the coil with a voltage step. When the coil goes normal, the current is dumped into a dump resistor. As far as the coil and coupled circuits are concerned, this is equivalent to a single turn-off pulse of the voltage, $V'(\tau)$, as illustrated in Fig. 7. There is no difference in the voltage and current at point a between the two circuits. The value of $V'(\tau)$ is $V'(\tau) = V(\tau) + I R_{dump}$. The only real difference is that the voltage that would be dropped across $I R_{dump}$ is saved by the switch, reducing the power required by the voltage source.

ORNL-DWG 75-10667

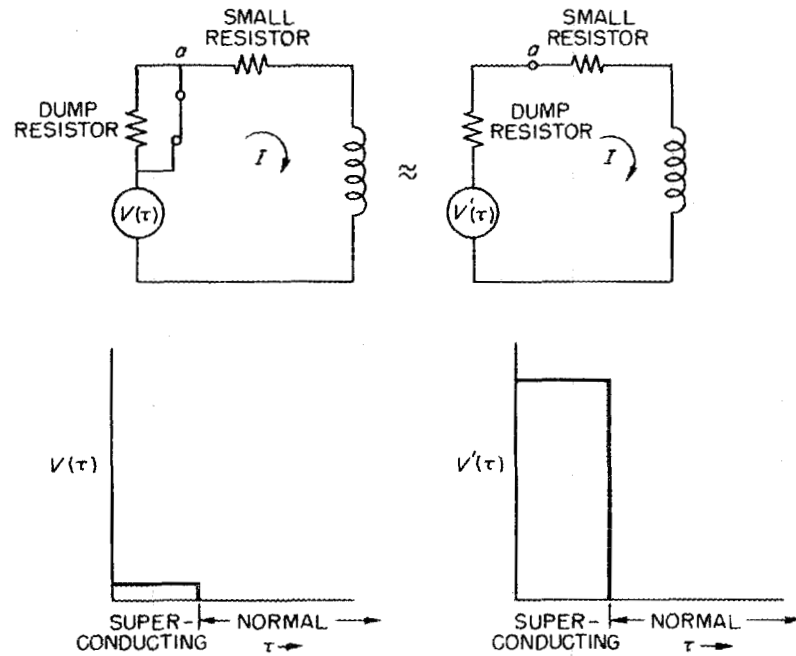


Fig. 7. Equivalent Dumping of Current in Coil.

Once the voltage functions, $V_q(\tau)$ are known or simulated, we can obtain the current coefficients, which in turn will give us the current in the various circuits. From these currents we can then calculate all of the other parameters, such as forces, eddy currents, and power dissipated.

IV. Measurements of the Various Properties

The calculated parameters can be measured with various degrees of accuracy and difficulty using models constructed of a similar material or liquid metals with probes inside them. We shall now discuss these measurements.

A. Eddy Current Density

This can be measured by putting a current probe in models containing mercury or Wood's metal. However, the current probe will upset the field to a certain extent in the region near the probe. The current is usually measured indirectly, using the voltage drop or the magnetic field.

B. Eddy Current Power

The total power can be determined by measuring the power consumed in the coil. The instantaneous power generated in a small section of the shielding can be determined by measuring temperature changes on the surface of the conductor using infrared techniques or by using the temperature coefficient of the metal's resistivity (measured with an eddy current probe) or by using thermocouples inside the metal. The latter measurement technique would probably influence the results more than the others, but it could be applied to the interior of the conductor. All three of these techniques depend on the shielding heating, which depends in turn on the geometry, thermal conductivity and heat capacity of the model.

C. Magnetic Field

The magnetic field can be measured using a Hall probe for both ac and dc fields or a pick-up coil for ac fields. The pick-up coil measures the time rate of change of the magnetic field that passes through the coil and furnishes both magnitude and phase information. The measurement accuracy will be about 1% for the pick-up coil. The Hall probe can measure the small fields to an accuracy of about 0.1%, with a frequency response from dc to about 20 KHz.

D. Force Density

The magnetic forces can be measured by measuring small displacements with strain gauges and extensometers, or by measuring the force required on a part to prevent the part from moving. The amount of displacement of a "rigid" body produced by a current pulse applied to a nearby coil will depend on the stress-strain relationships of the body and its inertia. Small, non-contacting eddy current displacement probes behind the part could measure a displacement up to 2000 μ in with a resolution of 1 μ inch and an accuracy of 10 μ inches, at a high vibrational frequency.

E. Voltages in Circuits

The magnitudes and phases of the voltages in the various circuits can be measured to within about 0.1% and 0.2°, respectively, at a particular sinusoidal frequency. These measurements will allow quite accurate calculations of the impedances and coupling coefficients in the various

circuits. The most accurate range of measurements is in the 50 Hz to 10 kHz range. The time-voltage relationship for a pulse can be measured to within about 1%, but it can probably be obtained more accurately using a Fourier sum of the various components to reconstruct the waveshape.

V. Use of Measurements and Scaling in Lieu of Calculations

There will be advantages and disadvantages to using either experimental measurements or numerical calculations. A list of several of these considerations is given below.

A. Advantages of Measurements

1. They will be required anyhow to verify the calculations.
2. In many instances the measurements will be more accurate than the calculations. In particular, for cases where we can use the results of a single frequency measurement, the measurements will be more accurate for quantities such as voltages, total impulse, and total power.
3. The measurements may point out problems and omissions made in the calculation.
4. The measurements may be cheaper than the 3-dimensional relaxations.

B. Advantages of Calculations

1. The calculations themselves will not introduce errors into the models as the measurements do.

2. It is the only way to obtain some answers, such as the force densities, eddy current densities and heating densities at various places inside the metal.
3. The calculations may give some special insights into the problem that the measurements would miss, such as where would be the best place to modify the specimen configuration to reduce the eddy currents.

In actual practice, the two techniques will probably complement each other to some extent.

VI. Experimental Verification of Scaling

There have been a number of experimental verifications of the scaling of induction problems. All of the standard eddy current calculations are scaled, with the scaling factors introduced as multipliers after all the numerical calculations have been performed using dimensionless functions. Therefore, any experimental verification of the calculations also verifies the scaling.

We have made a series of impedance measurements and calculations on coils of four different sizes and with different numbers of turns in the presence of conductors with the results shown in Table I.

The four coils varied in mean radius from 0.30 in. to 1.20 in., and the test frequency and liftoff were varied to keep the product $\omega\mu\sigma R_5^2$ and the normalized liftoff as nearly constant as possible. However, there were still variations, as shown by the standard deviations of the $\omega\mu\sigma R_5^2$ and liftoff, which contribute to the impedance variations. The

Table I. Normalized Coil Impedance for Four Coils from 0.30 to 1.20 in. Mean Radius as a Function of $\omega\mu\sigma R_5^2$ and Normalized Lift-off.

$\omega\mu\sigma R_5^2$	$S\bar{x}$	Lift-off	$S\bar{x}$	Measured				Calculated		% Difference	
				Im_n	$S\bar{x}$	$R1_n$	$S\bar{x}$	Im_n	$R1_n$	Im_n	$R1_n$
3.122	0.007	0.0473	0.0001	0.9990	0.0310	0.0766	0.0240	.9167	.1000	+8.98%	-23.40%
8.742	0.029			0.8250	0.0120	0.1312	0.0047	.8288	.1289	-4.59	+1.78
24.98	0.081			0.7343	0.0016	0.1300	0.0005	.7278	.1268	+8.93	+2.52
78.10	0.36			0.6427	0.0012	0.1029	0.0017	.6378	.1005	+7.68	+2.39
334.13	1.16			0.5703	0.0005	0.0610	0.0005	.5645	.0616	+1.03	-0.97
874.20	2.97			0.5364	0.0024	0.0437	0.0011	.5362	.0414	+0.04	+5.56
3.122	0.007	0.0946	0.0002	0.9175	0.0105	0.0692	0.0065	.9247	.0870	-0.78	-20.46
8.742	0.029			0.8410	0.0112	0.1066	0.0026	.8487	.1099	-0.09	-3.00
24.98	0.081			0.7693	0.0016	0.1086	0.0006	.7635	.1059	+0.76	+2.55
78.10	0.36			0.6917	0.0009	0.0845	0.0021	.6896	.0821	+0.30	+2.92
334.13	1.16			0.6339	0.0017	0.0488	0.0005	.6310	.0492	+0.46	-0.81
874.20	2.97			0.6070	0.0018	0.0351	0.0011	.6088	.0328	-0.30	+7.01
3.122	0.007	0.1892	0.0004	0.9225	0.0345	0.0480	0.0135	.9382	.0666	-1.67	-27.03
8.742	0.029			0.8693	0.0136	0.0817	0.0069	.8807	.0810	-1.29	+0.86
24.98	0.081			0.8245	0.0013	0.0830	0.0010	.8192	.0755	+0.65	+9.93
78.10	0.36			0.7707	0.0003	0.0593	0.0016	.7680	.0566	+0.35	+4.77
334.13	1.16			0.7735	0.0019	0.0326	0.0003	.7289	.0330	+6.12	-1.21
874.20	2.97			0.7140	0.0027	0.0229	0.0006	.7142	.0217	-0.03	+5.53
3.122	0.007	0.3785	0.0006	0.9870	0.0040	0.0292	0.0152	.9572	.0406	+3.11	-28.08
8.742	0.029			0.9293	0.0250	0.0538	0.0041	.9232	.0461	+0.66	+16.70
24.98	0.081			0.8933	0.0019	0.0478	0.0016	.8896	.0407	+0.42	+17.44
78.10	0.36			0.8647	0.0003	0.0322	0.0021	.8632	.0293	+0.17	+9.90
334.13	1.16			0.8470	0.0024	0.0164	0.0003	.8436	.0166	+0.40	-1.21
874.20	2.97			0.8382	0.0021	0.0115	0.0005	.8364	.0108	+0.22	+6.48

$S\bar{x}$ = standard deviation of the mean.

numbers of turns were all different, but were also eliminated by normalization. The impedances given in columns 5 and 7 are normalized by dividing by the coil inductance in air. The important quantities to notice in the table are the following: (1) the standard deviations of the real and imaginary parts of the normalized impedances (columns 8 and 6), which should be zero if the scaling, construction, and measurements were perfect; (2) the experimental and calculated values of the real and imaginary parts of the coil impedances for the various liftoffs (columns 7, 5, 10, 9). Note that, except for the first two values of $\omega\mu\sigma R_5^2$, for which the frequencies were so low that the measurements were not very accurate, the standard deviations in columns 6 and 8 are very small, indicating that the four different coils all gave the same results. This indicates the validity of the scaling laws which keep $\omega\mu\sigma R_5^2$ and the normalized liftoff constant and factor out the number of turns of the coils, when the driving coil and the pickup coil are one and the same. The calculated values in columns 9 and 10 are for a coil with normalized dimensions which are the average of those for the four coils. Since the percentage differences between measured and calculated values seem randomly scattered, it seems that the experimental measurements are most in error, and the variations are generally comparable to the standard deviations of the measurements.

Table II shows how the calculated and measured inductances vary for a large number of coils that have been used in a number of eddy current experiments, using the apparatus shown in Fig. 8. Although the agreement is quite good for these examples, there have been a few instances where the error was as large as 2%. It is suspected in these cases that an error occurred in the number of turns.

Table II. Comparison of Calculated and Measured Inductances

Mean radius \bar{r} (inches)	Inner Radius	Outer Radius	Length (inches)	Turns N	Inductance (Measured) mh	Inductance (Calculated) mh	% Difference
.603	.506	.700	.200	690	18.55	18.5185	+ .170
.603	.506	.700	.200	653	16.555	16.5857	- .185
.603	.506	.700	.200	1335	68.604	69.3218	-1.035
.60265	.5048	.7005	.208	435	7.319	7.26857	+ .702
.605375	.50525	.7055	.2094	445	7.564	7.60335	- .518
.56775	.5057	.6298	.201	285	3.157	3.16425	- .229
.60415	.5058	.7025	.200	1219	57.755	57.77024	- .026
.60335	.5063	.7004	.200	1219	57.77	57.84052	- .122
.60265	.5053	.7000	.200	1325	68.22	68.16977	+ .074
.49617	.333335	.65900	.333335	637	8.773	8.713	+ .689
.9951	.6666	1.3235	.6666	1404.7	85.658	84.89	+ .905
1.478	1.000	1.956	1.000	1212.3	94.30	94.24	+ .064
2.000415	1.333333	2.666749	1.333333	931	74.97	74.83	+ .187
.496	.333	.660	.333	637	8.863	8.712	+1.733
.998	.6666	1.3303	.6666	1404.8	85.94	85.09	+ .999
2.752	2.244	3.261	1.008	836	118	117.9	+ .777
2.748	2.244	3.248	1.005	835.3	117.5	116.93	+ .487
3.743	3.375	4.100	3.000	754	111.7	110.7	+ .903

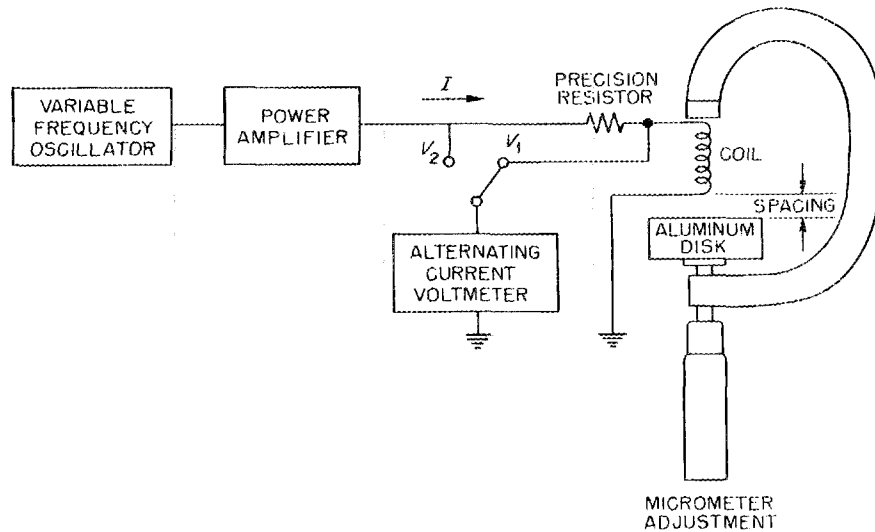


Fig. 8. Diagram of Impedance Measurement Apparatus.

In Table III we show the experimental force measurements for two different size coils with the same shapes, made with the apparatus illustrated in Fig. 9. These measurements again demonstrate the validity of scaling. The error is relatively large for these measurements, but they were made before more accurate experimental apparatus was available. Note that the forces are given in 10^{-7} newtons/(amp-turn)², indicating the validity of factoring out the number of turns and the driving current.

Table III. Comparison of Calculated and Measured Eddy Current Forces

$\omega\mu\sigma R_5^2$	Calculated Force*	Measured Coil B**	% Difference	Measured Coil C***	% Difference
Lift off = .0476 R_5 :					
3.082	1.12146	1.048	-6.55	1.058	-5.66
8.628	2.80859	2.642	-5.93	2.694	-4.08
24.65	5.11168	4.714	-7.78	4.954	-3.08
77.05	7.52462	6.933	-7.86	7.326	-2.64
329.8	9.82756	8.989	-8.53	9.664	-1.66
862.8	10.7935	10.18	-5.68	10.90	+0.99
Liftoff = .0952 R_5 :					
3.082	.987604	.9289	-5.94	.9540	-3.40
8.628	2.41421	2.265	-6.18	2.366	-2.00
24.65	4.29660	4.021	-6.41	4.260	-0.85
77.05	6.17141	5.776	-6.41	6.201	+0.48
329.8	7.85378	7.430	-5.40	7.954	+1.28
862.8	8.53364	8.237	-3.48	8.913	+4.46

* Forces in units of 10^{-7} newtons/(amp-turn)²

** Coil B mean radius = 0.6063 in.

*** Coil C mean radius = 0.9023 in.

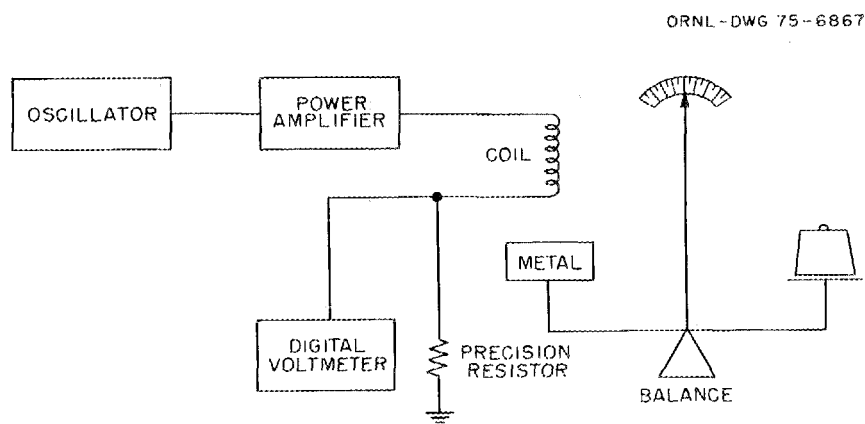


Fig. 9. Diagram of Force Measurement Apparatus.

VII. Summary and Conclusions

The concepts of scaling will allow experimental measurements made on relatively small models to be extended to full size models. There will be an optimum size for a model to obtain the most accurate results at the least expense. If the model is too small, it will be expensive to hold the coil and conductor dimensions to the desired tolerances, and the measuring apparatus will be difficult to install. On the other hand, if the model is too large, it will consume an expensive amount of materials and construction labor. A model which uses coils that are 2 to 4 inches in diameter would probably give the best results at the lowest cost.

The experimental measurements made thus far demonstrate the validity of scaling. However more accurate and additional measurements (such as the voltage coupling coefficients for multiple coils) need to be made to provide more confidence.

While the scaling can provide quite valuable design parameters, it will not furnish all of the answers. The best results will probably come from a balanced program of mathematical models and experimental models with comparisons between numerical calculations and experimental measurements.

References

1. C. V. Dodd, "Eddy-Current Impedance Calculated by a Relaxation Method," pp. 300-314 in *Proceedings of the Symposium on Physics and Nondestructive Testing*, Southwest Research Institute, San Antonio, Texas (1963).
2. C. V. Dodd, *A Solution to Electromagnetic Induction Problems*, ORNL-TM-1185 (August 1965). M.S. Thesis, The University of Tennessee.
3. C. V. Dodd, *Solutions to Electromagnetic Induction Problems*, ORNL-TM-1842 (June 1967). Ph.D. Thesis, The University of Tennessee.
4. J. Nelson Tunstall and C. V. Dodd, III, *A Computer Program to Solve Eddy-Current Problems*, K-1740 (April 8, 1968).
5. C. V. Dodd and W. E. Deeds, "Computer Design of Eddy-Current Tests," p. 199 in *Proceedings of Fifth International Conference on Nondestructive Testing*, Montreal, Canada, The Queen's Printer, Ottawa, Canada (1969).
6. C. V. Dodd, W. E. Deeds, and W. G. Spoeri, Optimizing Defect Detection in Eddy-Current Testing, *Materials Evaluation* 29, 59 (1971).

7. C. V. Dodd and W. A. Simpson, Jr., Measurements of Small Magnetic Permeability Changes by Eddy Current Techniques, *Materials Evaluation* 29, 217 (1971).
8. C. V. Dodd and W. A. Simpson, Jr., *Thickness Measurements Using Eddy-Current Techniques*, ORNL-TM-3712 (1972).
9. C. V. Dodd, C. C. Cheng, C. W. Nestor, and R. B. Hofstra, *Design of Induction Probes for Measurement of Liquid Metals*, ORNL-TM-4175 (1973).
10. C. V. Dodd, J. H. Smith, and W. A. Simpson, *Eddy-Current Evaluation of Nuclear Control Rods*, ORNL-TM-4321 (1973).
11. C. V. Dodd, W. E. Deeds, J. W. Luquire, and W. G. Spoeri, *Some Eddy-Current Problems and Their Integral Solutions*, ORNL-4384 (April 1969).
12. F. D. Mundt, *Eddy-Current Measurements with a Coil Encircling a Two-Conductor Rod*, Y-1787 (April 1971).
13. J. T. Hill, *Clad-Thickness Measurements Using Dual-Frequency Eddy Current*, Y-1970 (May 1974).
14. C. C. Feng, W. E. Deeds, and C. V. Dodd, Analysis of Eddy-Current Flowmeters, *Journal of Applied Physics* (July 1975).

ORNL-5077
UC-20 - Controlled Thermonuclear
Processes and Plasma Physics

INTERNAL DISTRIBUTION

- | | |
|------------------------------------|------------------------------------|
| 1-2. Central Research Library | 62. R. W. McClung |
| 3. Document Reference Section | 63. H. C. McCurdy |
| 4-6. Laboratory Records Department | 64. J. R. Miller |
| 7. Laboratory Records, ORNL R.C. | 65. A. R. Moazed |
| 8. ORNL Patent Office | 66. O. B. Morgan |
| 9-10. Thermonuclear Library | 67. J. W. Pearce |
| 11. W. C. Anderson | 68. H. Pih |
| 12. J. K. Ballou | 69. H. Postma |
| 13. R. L. Brown | 70. M. Roberts |
| 14. E. H. Bryant | 71. M. W. Rosenthal |
| 15. P. B. Burn | 72. R. E. Schwall |
| 16. W. D. Cain | 73. J. L. Scott |
| 17. D. D. Cannon | 74. T. E. Shannon |
| 18. J. F. Clarke | 75. S. S. Shen |
| 19. F. L. Culler | 76. J. E. Simpkins |
| 20. J. E. Cunningham | 77. W. A. Simpson |
| 21. R. W. Derby | 78. G. M. Slaughter |
| 22-41. C. V. Dodd | 79. D. Steiner |
| 42. G. W. Donaldson | 80. J. O. Stiegler |
| 43. L. Dresner | 81. W.C.T. Stoddart |
| 44. J. F. Ellis | 82. J. H. Smith |
| 45. W. A. Fietz | 83. P. B. Thompson |
| 46. A. P. Fraas | 84. D. B. Trauger |
| 47. K. F. Froelich | 85. P. L. Walstrom |
| 48. W. H. Gray | 86. J. R. Weir |
| 49. P. N. Haubenreich | 87. F. W. Wiffen |
| 50. R. F. Hibbs | 88. E. L. Woods |
| 51-53. M. R. Hill | 89. H. T. Yeh |
| 54. G. G. Kelley | 90. A. Zucker |
| 55. C. G. Lawson | 91. W. C. Leslie (consultant) |
| 56. C. J. Long | 92. John Moteff (consultant) |
| 57. H. M. Long | 93. Hayne Palmour III (consultant) |
| 58. J. K. Lovin | 94. J. W. Prados (consultant) |
| 59. M. S. Lubell | 95. N. E. Promisel (consultant) |
| 60. J. W. Lue | 96. G. V. Smith (consultant) |
| 61. J. N. Luton | 97. D. F. Stein (consultant) |

EXTERNAL DISTRIBUTION

98-99. USERDA DIVISION OF CONTROLLED THERMONUCLEAR RESEARCH, Washington,
DC 20545

Director

100-101. USERDA OAK RIDGE OPERATIONS OFFICE, P. O. Box E, Oak Ridge, TN
37830

Director, Reactor Division
Research and Technical Support Division

102-290. USERDA TECHNICAL INFORMATION CENTER, Office of Information
Services, P. O. Box 62, Oak Ridge, TN 37830

For distribution as shown in TID-4500 Distribution Category,
UC-20 - Controlled Thermonuclear Processes and Plasma Physics